Journal of Pharmaceutical Analysis 9 (2019) 91–99

Contents lists available at ScienceDirect

Journal of Pharmaceutical Analysis

journal homepage: www.elsevier.com/locate/jpa
www.sciencedirect.com

Original Article

Identification of α-glucosidase inhibitors from *Clinacanthus nutans* leaf extract using liquid chromatography-mass spectrometry-based metabolomics and protein-ligand interaction with molecular docking

Suganya Murugesu [a], Zalikha Ibrahim [a], Qamar Uddin Ahmed [a], Bisha Fathamah Uzir [a], Nik Idris Nik Yusoff [a], Vikneswari Perumal [b], Faridah Abas [c], Khozirah Shaari [c], Alfi Khatib [a,c,*]

[a] *Department of Pharmaceutical Chemistry, Kulliyyah of Pharmacy, International Islamic University Malaysia, 25200 Kuantan, Pahang Darul Makmur, Malaysia*
[b] *Department of Pharmaceutical Technology, Faculty Pharmacy & Health Sciences, Universiti Kuala Lumpur, Royal College of Medicine Perak, 30450 Ipoh, Perak Darul Ridzuan, Malaysia*
[c] *Laboratory of Natural Products, Institute of Bioscience, Universiti Putra Malaysia, 43400 Serdang, Selangor Darul Ehsan, Malaysia*

ARTICLE INFO

Article history:
Received 28 February 2018
Received in revised form
13 November 2018
Accepted 14 November 2018
Available online 15 November 2018

Keywords:
Clinacanthus nutans
LC-MS-QTOF
Metabolomics
α-Glucosidase inhibitors
Diabetes
Molecular docking

ABSTRACT

The present study used *in vitro* and *in silico* techniques, as well as the metabolomics approach to characterise α-glucosidase inhibitors from different fractions of *Clinacanthus nutans*. *C. nutans* is a medicinal plant belonging to the Acanthaceae family, and is traditionally used to treat diabetes in Malaysia. *n*-Hexane, *n*-hexane: ethyl acetate (1:1, v/v), ethyl acetate, ethyl acetate: methanol (1:1, v/v), and methanol fractions were obtained via partitioning of the 80% methanolic crude extract. The *in vitro* α-glucosidase inhibitory activity was analyzed using all the fractions collected, followed by profiling of the metabolites using liquid chromatography combined with mass spectrometry. The partial least square (PLS) statistical model was developed using the SIMCA P^{+} 14.0 software and the following four inhibitors were obtained: **(1)** 4,6,8-Megastigmatrien-3-one; **(2)** N-Isobutyl-2-nonen-6,8-diynamide; **(3)** 1′,2′-bis(acetyloxy)-3′,4′-didehydro-2′-hydro-β, ψ-carotene; and **(4)** 22-acetate-3-hydroxy-21-(6-methyl-2,4-octadienoate)-olean-12-en-28-oic acid. The *in silico* study performed via molecular docking with the crystal structure of yeast isomaltase (PDB code: 3A4A) involved a hydrogen bond and some hydrophobic interactions between the inhibitors and protein. The residues that interacted include ASN259, HID295, LYS156, ARG335, and GLY209 with a hydrogen bond, while TRP15, TYR158, VAL232, HIE280, ALA292, PRO312, LEU313, VAL313, PHE314, ARG315, TYR316, VAL319, and TRP343 with other forms of bonding.

1. Introduction

Regulating hyperglycemic conditions with modern medicine or herbal remedies is a therapeutic method that can be used to manage type-2 diabetes mellitus (DM). Many natural resources have been investigated for their ability to suppress the glucose production from carbohydrates in the gut, or absorption of glucose from the intestines [1]. Typically, type-2 DM is described as a metabolic disorder associated with hyperglycaemia and an increased blood glucose level, which results in damages to the human body. Presently, type-2 DM is regarded as the major leading cause of mortality, and is referred to as an epidemic as the number of cases continues to increase epidemically [2]. Medicinal plants have been used traditionally in diabetes management. Nowadays, many researches performed are focused on the use of medicinal plants as an alternative form of type-2 DM management. Medicinal plants consist of a complex mixture of phytoconstituents that enables them to exhibit their medicinal properties through synergistic actions [3].

Clinacanthus nutans (*C. nutans)* (Burm. F) Lindau, a medicinal shrubcommonly known as Sabah snake grass, belongs to the diverse family of Acanthaceae. This group of flowering plants can easily grow in many different habitats such as bushes, forests, swamps and mangrove areas. *C. nutans* is native to Malaysia, China, Indonesia, as well as Thailand, and is widely distributed in the locality of these countries. Many scientific studies have demonstrated the therapeutic potential of *C. nutans* including its antiviral, anti-inflammatory, antioxidant, neuromodulatory and

Peer review under responsibility of Xi'an Jiaotong University.
* Corresponding author at: Department of Pharmaceutical Chemistry, Kulliyyah of Pharmacy, International Islamic University Malaysia, 25200 Kuantan, Pahang Darul Makmur, Malaysia.
E-mail address: alfikhatib@iium.edu.my (A. Khatib).

https://doi.org/10.1016/j.jpha.2018.11.001

anti-cancer properties. Since ancient times, its leaf extract has been traditionally applied as a tropical treatment for skin rashes, snake bites, and allergic reactions. Traditionally, the leaf of *C. nutans* is often consumed to treat diabetes and diuresis [4]. The traditional medicinal practitioners, especially in Indonesia and Thailand, commonly prepare herbal medicines from *C. nutans* using the decoction method; the resulting formulation is then used to treat multiple conditions including dysuria, diabetes, and hyperuricemia [4,5]. Lee et al. [6] conducted an anti-diabetes analysis via an *in-vitro* bioassay to analyze the α -glucosidase inhibitory activity of the plant's methanolic extract, and the results showed that the leaf and stem extracts exhibit a mild inhibition ($IC_{50} > 100\,\mu g/mL$). However, this study serves as the only evidence for the activity of other solvent extracts or compound (s) responsible for the activity reported. The present study has aimed at providing evidence of the effectiveness of the *C. nutans* extract against hyperglycaemia. To explore the efficacy of *C. nutans* against hyperglycaemia, we employed an *in vitro* technique against α-glucosidase.

In this study, we utilized liquid chromatography (LC) coupled with quadrupole time-of-flight (Q-TOF) mass spectrometry (MS) to technically identify compounds that correspond to the bioactivity. LC-MS Q-TOF provides high resolution in separation, and high sensitivity and reproducibility when the complexity of a plant mixture is examined [7]. In addition, the instrument aids in the detection of very low-abundant metabolites in the presence of compounds that are more vastly abundant. Notably, mass fragmentation is an added advantage of using MS Q-TOF, as it functions as a mining tool for profiling. Thus, a comprehensive suite of metabolomics data is provided to ease identification and pathway elucidation. Furthermore, being able to obtain the fragmentation profile data for compounds aids in the identification of a wide range of compounds present in the plant. In most studies, the biological activities are screened for the individual compounds present, upon isolation; thus, the biological effects of these compounds are often overlooked within the complex matrix of the leaves. A synergistic effect between the components may play a role in the bioactivity exhibited in the plant matrix. Therefore, an individual compound isolated may not be responsible for the observed bioactivity of the plant. This type of data analysis can however be achieved using the metabolomics approach associated with multivariate data analysis, which aids in determining the metabolites responsible for the observed bioactivity [8].

The current study presents the results of an *in silico* study of the molecular interaction between the enzymes' homology model and the inhibiting compounds (ligands) identified in the leaf extracts from *C. nutans*. The ligand-protein interaction can be predicted and virtually visualized using the ligand-protein complex, which displays the binding of the inhibitors to the protein receptor [9]. The aims of this study were to evaluate the α-glucosidase inhibitory activity of different leaf fractions from *C. nutans in vitro* and *in silico*, and to identify the related bioactive compounds in the fractions using LC-MS-based metabolomics.

2. Materials and methodology

2.1. Materials

Organic chemicals of analytical and chromatography grade were purchased from Merck (Darmstadt, Germany). The substrate, ρ-Nitrophenyl-ρ-D-glucopyranosidase (PNPG), and N-methyl-N (trimethylsilyl) trifluoroacetamidepurum (97.0%) (Chromatography grade) were obtained from Sigma-Aldrich (St. Louis, Missouri, USA). The α-glucosidase (yeast maltase) enzyme was obtained from Megazyme (Ireland).

2.2. Sample collection

The plant material (an estimated 7 kg) was obtained from Ees Biotech Sdn. Bhd. (Bukit Mertajam, Penang, Malaysia). A whole-plant sample was submitted for authentication to the Herbarium at the International Islamic University Malaysia, Kuantan Campus, Malaysia, where the specimen voucher number obtained was PIIUM 0238–1. Leaves harvested were washed with water and dried under a shade at 25 °C (± 0.5 °C) for a week. The dried leaves were converted to powder using a universal cutting mill (Fritsch, Germany) and were stored at − 80 °C prior to extraction [10].

2.3. Preparation of extract

The dried leaves (6.02 kg) were subjected to maceration in 80% methanol solution in a 1:3 (w/v) ratio for 3 days. Changing of the solvent was performed each day and was filtered with Whatman filter paper No.1. The solvent was then dried using a rotary evaporator under reduced pressure at 40 °C. The obtained crude extract (1.46 kg, yield = 24.3% [w/w]) was further macerated using different solvents in a polarity increasing manner, ranging from *n*-hexane (H), *n*-hexane:ethyl acetate (HE) (1:1, v/v), ethyl acetate (E), ethyl acetate:methanol (EM) (1:1, v/v) and methanol (M), with a sample to solvent ratio of 1:3 (w/v). All fractions were prepared in six replications and were recovered and stored at − 80 °C prior to analysis [11,12]. All fractions were tested using an α-glucosidase inhibitory activity assay and analyzed using the Q-TOF LC-MS instrument [10,13].

2.4. α-Glucosidase inhibition assay

The α-glucosidase inhibitory activity assay was performed using the method described by Javadi et al. [10]. Quercetin, a known α-glucosidase enzyme inhibitor, was used as the positive control and PNPG used as the substrate. The enzyme was prepared by dissolving 1 mg quercetin in 1 mL of methanol, while 6 mg of the substrate was dissolved in 20 mL of a 50 mM phosphate buffer (pH 6.5). The assay was conducted in a 96-well plate, which contained 10 μL of the samples, quercetin, and negative control (solvent). The wells containing samples and control were treated with 100 μL of 30 mM phosphate buffer and 15 μL of 0.02 U/μL α-glucosidase from *Saccharomyces cerevisiae* (Megazyme, Ireland); the well containing blank consisted of 115 μL of buffer without the enzyme. After a 5 min incubation at room temperature, the wells containing sample and blank were treated with 75 μL of PNPG. Finally, the reaction was stopped using glycine (pH 10) after an additional 15 min incubation. The amount of ρ-nitrophenol released from PNPG was measured using a microplate reader (TecanNanoquant Infinite M200, Switzerland) at a wavelength of 405 nm. The half-maximal inhibition concentration (IC_{50}), which depicted the concentration of inhibitor required to produce 50% inhibition of the enzymatic reaction at a specific substrate concentration [14], was determined using linear regression analysis. All analyzes were performed in triplicates, and the inhibitory activity (%) of each fraction was calculated using the following formula:

$$\text{Inhibitory activity}(\%) = \left[\left(A_{control} - A_{sample}\right)/A_{control}\right] \times 100\%$$

where $A_{control}$ is the absorbance of the negative control, and A_{sample} is the absorbance of the sample or positive control.

2.5. LC-MS analysis

LC-MS was used to detect the metabolites present in the leaf fractions from *C. nutans*, as described by Lawal et al. [13] with

slight modifications. The samples were analyzed using the Q-TOF LC-MS system, Agilent 1290 Infinity, and 6550 iFunnel Q-TOF LC/MS (Agilent Technologies, Santa Clara, California) equipped with an electrospray (ESI) interface comprising both positive and negative ion modes. Approximately 2 mg of each fraction was dissolved in 200 μL methanol, filtered and then transferred to the glass vials. The samples were injected on a Phenomenax Kinetex C_{18} core-shell technology 100 Å (250 mm × 4.6 mm, 5 μm) column that was previously flushed with methanol. Samples were eluted with a gradient system from 5% methanol in water with 0.1% formic acid, to absolute methanol in 10 min; the system was then maintained with absolute methanol for another 10 min at a flow rate of 0.7 mL/min with a total acquisition time of 30 min. All metabolites eluted were detected by Q-TOF MS operated in ESI at positive mode. The MS/MS data were collected in the range of 100–1700 *m/z* with a scan rate of 1 spectra/scan. The MS/MS spectra were obtained by a collision energy ramp of 30–35 eV.

All the LC-MS data acquired were analyzed using ACD/Spec Manager v.12.00 (Advanced Chemistry Development, Inc., ACD/Labs Toronto, Canada). The raw (*.xms) files were subsequently converted to net CDF (*.cdf) format using ACD/Spec manager. The LC-MS data were then pre-processed using the MZmine software (VTT Technical Research Centre, Finland) [15] for peak filtering, peak identification, peak matching, retention time correction and peak filing; the result was then saved as a (*.csv) file. The detected peak list was generated using the average area, corrected retention time and mass over charge (*m/z*) data as the identifiers for the various peaks.

2.6. Molecular docking

Molecular docking studies were performed to understand the binding modes of proteins with the identified inhibitors using AutoDock Tools (version 1.5.6). *Saccharomyces cerevisiae* isomaltase (SCI) (PDB code: 3A4A) α-glucosidase crystal structures were obtained from protein data bank (PDB). The protein structure is built with its potent and selective inhibitor, α-D-glucose (ADG), at a resolution of 1.6 [16]. The 3D structure of the positive control (quercetin) and the identified compounds were obtained from the Chemspider (Raleigh, North Carolina, USA) and Super Natural II databases [17]. The files were converted to (*.pdb) using Biovia Discovery Studio (San Diego, USA) prior to docking. A Lamarckian genetic algorithm (GA) method of 50 runs was used for docking. Gasteiger charges were added by default, while the rotatable bonds were set using AutoDock Tools; all torsions could be rotated. Grid box size was set to the maximum with default spacing. The grid box parameters for X, Y, and Z centers were 21.272, − 0.751 and 18.633, respectively [16,18–20]. To mimic the actual condition of the observed bioassay, the crystal structure of the enzyme was protonated as per the assay condition, with a pH of 6.5 using PDB2PQR Server, version 2.0.0 [19]. The 3D superimposed diagram of quercetin and the compounds was generated using PyMOL™ 1.7.4.5 (Schrödinger, LLC, NY, USA).

2.7. Data processing and statistical analysis

The significant value of the data was evaluated using Minitab 17 (Minitab Inc., State College, PA) and the ANOVA analysis of Tukey's test comparison with $p < 0.05$. All data are represented as mean ± standard deviation (SD), with a total of six replicates. Meanwhile, the multivariate data analysis (MVDA) was conducted using the SIMCA P+14.0 software (Umetrics, Umeå, Sweden) using Partial Least Square (PLS) where the UV scaling method was applied.

3. Results

3.1. α-Glucosidase inhibitory activity

The IC_{50} values for the α-glucosidase inhibitory activity were obtained for all leaf fractions from the *C. nutans* plant (Table 1). A higher inhibitory activity is observed when a lower IC_{50} value (< 50 μg/mL) is observed [21]. The *n*-hexane fraction exhibited the highest α-glucosidase inhibitory activity with an IC_{50} value of 3.07 μg/mL, while the methanol fraction exhibited the lowest activity with an IC_{50} value of 133 μg/mL. The results depict that a decrease in inhibitory activity occurs with increasing fraction polarity.

3.2. Multivariate data analysis

Multivariate data analysis was used to correlate the bioassay activity and the analyzed spectra. This was in efforts to identify the potential inhibitors present in the fractions. By using the discriminant analysis, the PLS model was performed to discriminate among the fractions, and to pinpoint the mass to charge (*m/z*) ratio values that were contributing to the bioactivity [10]. The variables were fitted automatically using 2 principal components, PLS components 1 and 2, with the *m/z* of specific retention times extracted using positive ionization. The IC_{50} values of each sample were deemed x and y variables, respectively. The goodness of fit for the model was based on the cumulative values; where R^2Y indicated the percentage of variation of the response explained by the model, and Q^2Y represented the percentage of variation in the response predicted by the model (based on cross validation). In this study, the R^2Y and Q^2Y values were 0.95 and 0.87, respectively. Therefore, the fitness of the model and the predictive ability were considered good when the cumulative values of both R^2Y and Q^2Y were greater than 0.5 [22].

The performance and accuracy of the model were measured based on the root-mean-square errors of estimation ($RMSE_E$) which calculates the average deviation of the model from the data. Performance and accuracy were also measured via the root-mean-square error of cross-validation ($RMSE_{CV}$), which is a measure of the quality of the model in predicting new samples. A lower $RMSE_{CV}$ value indicated a higher predictive accuracy for the new samples. As per this model, the $RMSE_E$ and the $RMSE_{CV}$ values were 0.01 and 0.02, respectively.

Fig. 1A shows the score scatter plot of the fractions generated using the LC-MS positive ionization. The plot displays the distribution of the variables based on PLS components 1 and 2, and clearly separates the active and less active fractions from *C. nutans* leaves. Based on PLS component 1, the active fraction H, is well distributed in the positive quadrant; the other fractions were located in the negative quadrant. Fig. 1B shows the loading scatter plot of the different fractions of the leaf crude extracts from *C. nutans* using the positive ionization mode in the LC-MS analysis.

Table 1
The half maximal inhibitory concentration (IC_{50}) of the α-glucosidase inhibitory activity of the *C. nutans* leaf fractions.

Solvent fraction	IC_{50} (μg/mL, mean ± SD)
n-Hexane (H)	3.07 ± 0.05^{d}
n-Hexane: ethyl acetate (HE)	5.54 ± 0.09^{d}
Ethyl acetate (EA)	8.42 ± 0.17^{c}
Ethyl Acetate: Methanol (EM)	37.45 ± 0.90^{b}
Methanol (M)	133.57 ± 0.30^{a}
Quercetin	5.77 ± 1.01

Means that do not share the same letter are significantly different with *p* value < 0.05.
SD = Standard Deviation. $n = 6$.

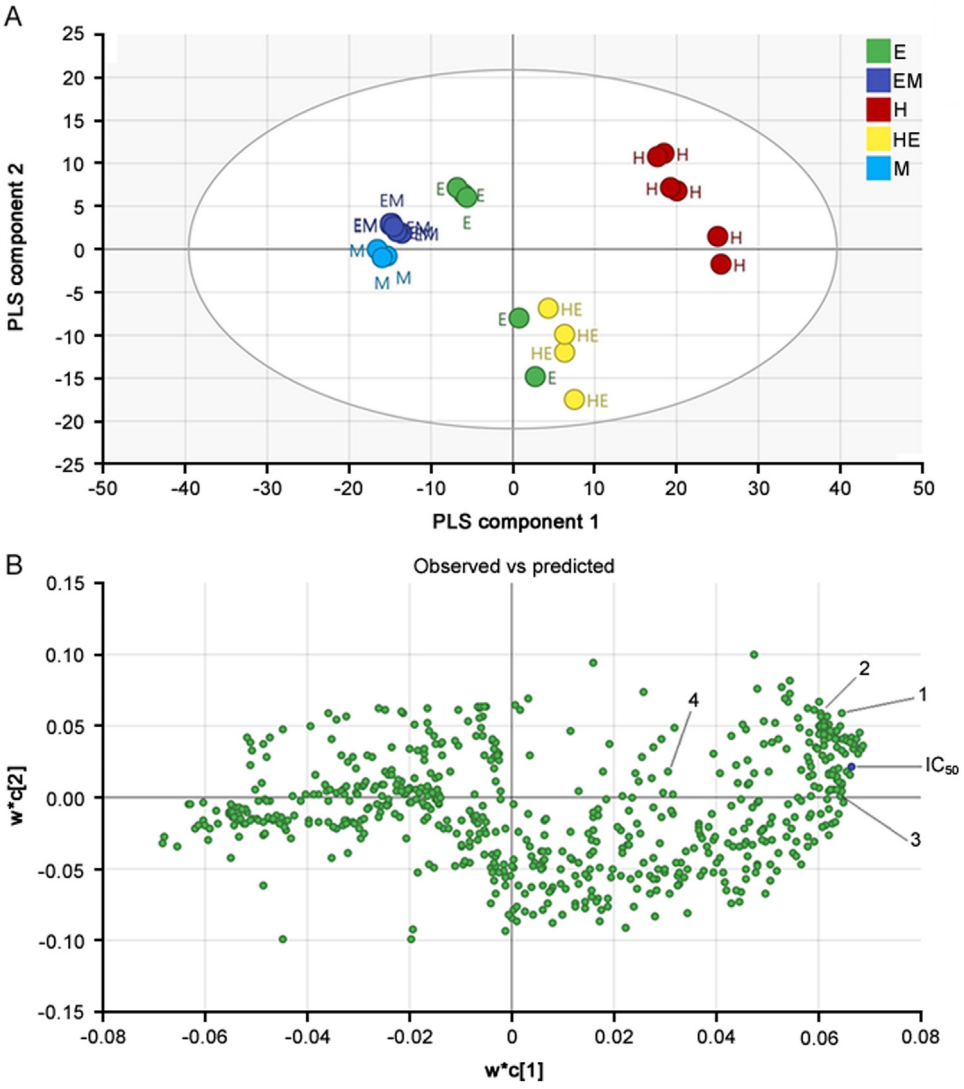

Fig. 1. (A) PLS score scatter plot of different solvent fractions from the *C. nutans* leaves using positive ionization in the LC-MS analysis. H, *n*-hexane; HE, *n*-hexane: ethyl acetate; E, ethyl acetate; EM, ethyl acetate: methanol and M, methanol. (B) The loading scatter plot of the PLS model of the fractions analyzed using LC-MS with positive ionization. The identified α-glucosidase inhibitors are: (**1**) 4,6,8-Megastigmatrien-3-one; (**2**) N-Isobutyl-2-nonen-6,8-diynamide; (**3**) 1′,2′-bis(acetyloxy)-3′,4′-didehydro-2′-hydro-β, ψ-carotene; and (**4**) 22-acetate-3-hydroxy-21-(6-methyl-2,4-octadienoate)-olean-12-en-28-oic acid.

The metabolites labelled near the IC_{50} value in Fig. 1B, are those measured to be positively correlated with the α-glucosidase inhibiting activity. In addition, the PLS model was validated based on the observed versus predicted plot, and the regression equation used to measure its validation; the R^2 value was 0.9891. The prediction model is valid when R^2 is greater than 0.9 [22].

Table 2
Tentative metabolites identified in the *C. nutans* leaves fractions through LC-MS/MS fragmentation using positive ionization.

Compound	M+H	MS^2 fragments ions	Tentative metabolites	Refs.
1	191.2	$[M\text{-}CHO]^+$ at *m/z* 161, $[M\text{-}C_3H_5]^+$ at *m/z* 149, $[M\text{-}C_2H_3O]^+$ at *m/z* 147, $[M\text{-}C_2H_5O]^+$ at *m/z* 145, $[M\text{-}C_2H_6O]^+$ at *m/z* 144, $[M\text{-}C_2H_7O]^+$ at *m/z* 143, $[M\text{-}C_4H_7]^+$ at *m/z* 135, $[M\text{-}C_3H_5O]^+$ at *m/z* 133, $[M\text{-}C_3H_7O]^+$ at *m/z* 131, $[M\text{-}C_3H_9O]^+$ at *m/z* 129, $[M\text{-}C_3H_{10}O]^+$ at *m/z* 128, $[M\text{-}C_4H_5O]^+$ at *m/z* 121, $[M\text{-}C_4H_7O]^+$ at *m/z* 119, $[M\text{-}C_4H_9O]^+$ at *m/z* 117, $[M\text{-}C_4H_{10}O]^+$ at *m/z* 116, $[M\text{-}C_4H_{11}O]^+$ at *m/z* 115, $[M\text{-}C_5H_5O]^+$ at *m/z* 109, $[M\text{-}C_5H_7O]^+$ at *m/z* 107, $[M\text{-}C_5H_8O]^+$ at *m/z* 106 and $[M\text{-}C_5H_9O]^+$ at *m/z* 105	4,6,8-Megastigmatrien-3-one	[22–24]
2	204.1	$[M\text{-}C_2H_5]^+$ at *m/z* 174, $[M\text{-}C_2H_5N]^+$ at *m/z* 160, $[M\text{-}C_3H_2O]^+$ at *m/z* 149, $[M\text{-}C_4H_7]^+$ at *m/z* 148, $[M\text{-}C_5H_6O]^+$ at *m/z* 121, $[M\text{-}C_5H_9N]^+$ at *m/z* 120, $[M\text{-}C_6H_{10}O]^+$ at *m/z* 105, $[M\text{-}C_6H_{11}O]^+$ at *m/z* 104 and $[M\text{-}C_6H_{12}O]^+$ at *m/z* 103	N-Isobutyl-2-nonen-6,8-diynamide	[25–27]
3	653.5	$[M\text{-}C_5H_9O]^+$ at *m/z* 567, $[M\text{-}C_5H_{10}O]^+$ at *m/z* 566, $[M\text{-}C_4H_7O_2]^+$ at *m/z* 565, $[M\text{-}C_4H_{11}O_2]^+$ at *m/z* 561, $[M\text{-}C_5H_9O_2]^+$ at *m/z* 551, $[M\text{-}C_6H_{11}O_2]^+$ at *m/z* 537, $[M\text{-}C_7H_{13}O_3]^+$ at *m/z* 507 and $[M\text{-}C_8H_{13}O_4]^+$ at *m/z* 479	1′,2′-bis(acetyloxy)-3′,4′-didehydro-2′-hydro-β, ψ-carotene	[28]
4	667.5	$[M\text{-}C_{17}H_{25}O_4]^+$at *m/z* 373, $[M\text{-}C_{21}H_{33}O_3]^+$ at *m/z* 333, and $[M\text{-}C_{19}H_{25}O_6]^+$ at *m/z* 317	22-acetate-3-hydroxy-21-(6-methyl-2,4-octadienoate)-olean-12-en-28-oic acid	[17]

3.3. Structure elucidation using a fragmentation pathway

Elucidating the chemical structure of each parent ion was performed through MSMS fragmentations. The identification of each metabolite was confirmed by comparing it to the published reports or databases such as ACD Lab, Inc. (Toronto, Canada), and by analyzing the ion fragmentation patterns. The summary of the fragmentation is displayed in Table 2 [17,22–28]. The metabolites identified are: (1) 4,6,8-Megastigmatrien-3-one; (2) N-Isobutyl-2-nonen-6,8-diynamide; (3) 1′,2′-bis(acetyloxy)-3′,4′-didehydro-2′-hydro-β, ψ-carotene; and (4) 22-acetate-3-hydroxy-21-(6-methyl-2,4-octadienoate)-olean-12-en-28-oic acid. Meanwhile, the chemical structures of the α-glucosidase inhibitors are illustrated in Fig. 2.

Compound **1** is essentially a cyclic ketone with its carbonyl functional group at C3, alkyl groups at C1 and C5 and three C=C at positions 4, 6 and 8. In the positive ionization mode (ESI), compound **1** was protonated at the C=O functional group located at C3 to form the parent ion $(M+H)^+$ having an *m/z* of 191. Cyclic rearrangement and removal of CH_2O, C_3H_6, C_2H_4O, C_4H_8, C_3H_6O, C_4H_6O, C_4H_8O, C_5H_6O, C_5H_7O, and $C_5H_{10}O$ from the parent ion produced ions with *m/z* of 161,149, 147, 135, 133, 121, 119, 109, 107, and 105, respectively. The loss of water from the ion with an *m/z* of 149 led to the formation of the ion having an *m/z* of 131; the loss of methyl resulted in the formation of the ion with an *m/z* of 116. The loss of C_4H_6O from the parent ion produced the ion with an *m/z* of 121, which was followed by the loss of methyl to form the ion with an *m/z* of 106. In addition, the loss of water from the parent ion led to the formation of the ion with an *m/z* of 173; this was further fragmented to the ion with an *m/z* of 117 due to the loss of C_4H_8. The loss of methyl from the ion with an *m/z* of 173 formed the ion having an *m/z* of 158; this was further fragmented to the ion with an *m/z* of 144 via loss of CH_2. The loss of C_2H_5 from this ion resulted in the formation of the ion with an *m/z* of 115. Deprotonation of the ion with an *m/z* of 173 formed the ion with an *m/z* of 172; this was subsequently fragmented to ions with *m/z* of 143, 129, and 128, due to the loss of C_2H_5, CH_2, and H, respectively. Lastly, the deprotonation of the parent ion resulted in the formation of the ion with an *m/z* of 190, which further fragmented to the ion with an *m/z* of 145 through the loss of C_2H_5O; this was then deprotonated to form the ion with an *m/z* of 144.

Compound **2** (*m/z*, 204; $[M+H]^+$) consists of an amide group where the N is attached to the long chain of the alkyl group. The protonation of compound **2** at the C=O attached to its amide group at C1 formed the parent ion $(M+H)^+$ with an *m/z* of 204. Production of the ion with an *m/z* of 174 occurred by the removal of a C_2H_6 from the alkyl chain of the parent ion. While the removal of methyl from the parent ion formed the ion with an *m/z* of 189, further fragmentation resulted in the loss of CH_3N to produce an ion with an *m/z* of 160. The subsequent loss of C_3H_3O and C_3H_8 from the parent ion formed the ions with *m/z* of 149 and 105, respectively. The loss of C_3H_4O from the parent ion resulted in the formation of the ion with an *m/z* of 148; this was fragmented to the ion with an *m/z* of 104 by the removal of the propyl group. Further fragmentation of this ion led to an ion with an *m/z* of 103 due to deprotonation at C5. While the removal of CH_2N from the ion with an *m/z* of 148 formed the ion with an *m/z* value of 120, the subsequent loss of C_2H_2 and C_3H_4O from the parent ion formed the ion with an *m/z* of 122, which was deprotonated to form the ion with an *m/z* of 121.

Compound **3**, a carotenoid with more than 40 carbons in its structure, contains a bis-acetyloxy group that shares a carbon with an alkyl group. During positive ESI, compound **3** was protonated at one of the oxygen atoms attached to the acetyloxy group to form the parent ion $(M+H)^+$ with an *m/z* of 653. Subsequent removal of CH_4, C_2H_2, methyl, and CHO from this ion resulted in ions with *m/z* of 637, 611, 596, and 567, respectively. The loss of methyl from the ion with an *m/z* of 637 produced with *m/z* 622 ion, which underwent rearrangement prior to fragmentation to form the ion with an *m/z* of 605, by HO removal. The loss of C_2H_4O from this ion produced the ion with an *m/z* of 561. The loss of C_3H_8 from the parent ion resulted in the formation of the ion with an *m/z* of 609; this was further fragmented to the ion with an *m/z* of 566 by the loss of C_2H_3O. In another pathway, the parent ion lost C_2H_4O to form the ion with an *m/z* of 609; this was further fragmented to ions with *m/z* of 594 and 507, after removal of methyl and $C_5H_{10}O_2$, respectively. A further fragmentation of the ion with an *m/z* of 594 produced the ion with an *m/z* of 565 by the loss of CHO. Meanwhile, a subsequent loss of $C_5H_{10}O_2$ and CH_2 resulted in the formation of ions with *m/z* of 551 and 537, respectively. Finally, the removal of $C_8H_{14}O_4$ from the parent ion formed the ion with an *m/z* of 479.

Compound **4** is a cyclic terpene with hydroxyl, carboxylic acid, and ester groups. Protonation of this compound occurred at the oxygen attached to the ester group produced from the parent ion $(M+H)^+$, with an *m/z* of 667. The removal of $C_{17}H_{26}O_4$ and $C_{19}H_{26}O_6$ from this ion resulted in the formation of ions with *m/z* of 373 and 317, respectively. A subsequent removal of CH_2O_2, $C_{19}H_{30}O$, and CH_2 from the parent ion resulted in ions with *m/z* of 621, 347, and 333, respectively.

3.4. LC-MS profiling

All identified metabolites were confirmed by scrutinizing the spectral pattern and comparing to ACD Lab, Inc. (Toronto, Canada) databases and journal reports. The four metabolites identified are labelled and shown in the chromatogram of each of the fraction analyzed and displayed in Fig. 3. From the spectra, the compounds were abundantly observed in the H, HE and E fractions, and were

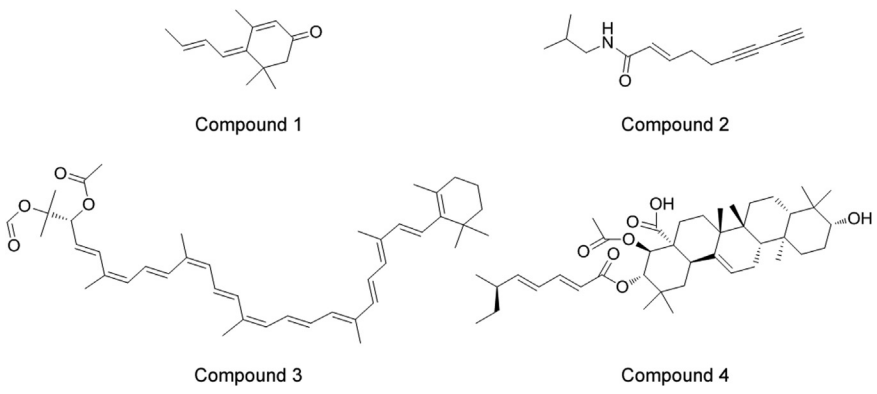

Fig. 2. The bioactive compounds that inhibit α-glucosidase enzyme activity. (1) 4,6,8-Megastigmatrien-3-one; (2) N-Isobutyl-2-nonen-6,8-diynamide; (3) 1′,2′-bis(acetyloxy)-3′,4′-didehydro-2′-hydro-β, ψ-carotene; and (4) 22-acetate-3-hydroxy-21-(6-methyl-2,4-octadienoate)-olean-12-en-28-oic acid.

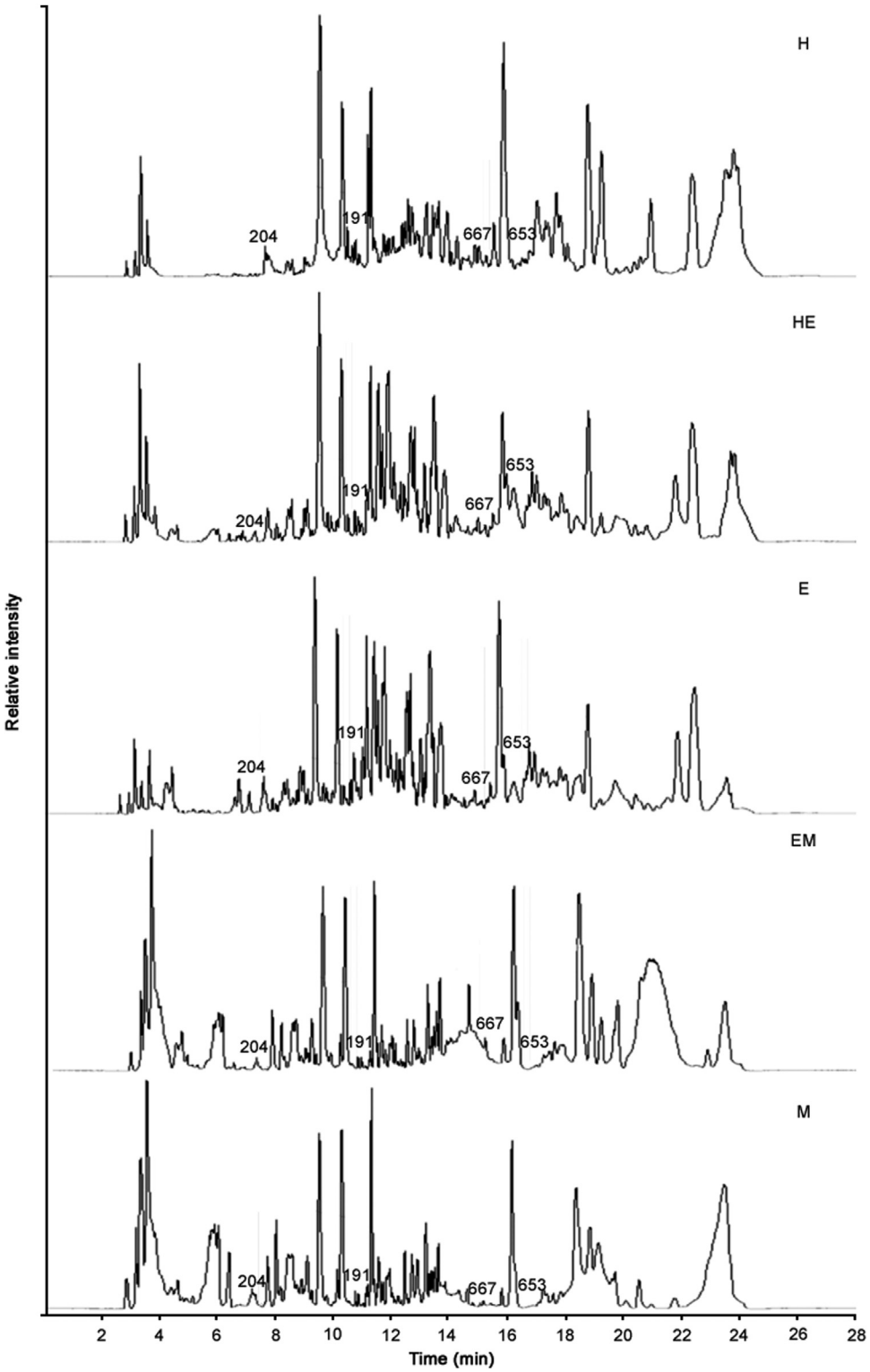

Fig. 3. The LC-MS spectra of all labelled with the mass of the compounds identified. H, *n*-hexane; HE, *n*-hexane: ethyl acetate; E, ethyl acetate; EM, ethyl acetate: methanol; and M, methanol.

less in the EM and M fractions. This indicates that the hydrophobicity of the compounds makes them more likely to be better represented in less polar fractions.

3.5. Molecular docking

Table 3 displays the binding energy of the compounds with the interacting residues. The control ligand simulation is meant to validate the docking simulation conducted. Meanwhile, the positive control, quercetin was analyzed for comparison to the compounds. From the docking results, one of the compounds identified using LC-MS showed a potentially lower binding energy than that of the positive control; at rest, the measured energy level was comparable to the control ligand. This indicates the binding affinity of the metabolites to the protein chains. Compound **1** was found to interact with ASN259, and HID295 via hydrogen bonding

Table 3
Molecular interaction results of α-glucosidase enzymatic protein with the known inhibitor (Quercetin) and the active compounds quantified using LC-MS.

Compound	Binding energy (kcal/mol)	H-bond interacting residues	Other interacting residues
Control ligand	− 6.00	ASH69, HIE112, GLN182, ARG213, ASH215, GLH277, HIE351, ASP352, ARG442	TYR72
Quercetin	− 8.15	LYS156, THR310, PRO312, LEU313, GLU411, ASN415	PHE314, ARG315
1	− 7.47	ASN259, HID295	TRP15, ALA292, TRP343
2	− 5.54	LYS156	TYR158, VAL232, VAL313
3	− 10.19	ARG335	LYS156, TYR158, PRO312, PHE314, ARG315, TYR316
4	− 8.31	GLY209	VAL232, HIE280, VAL308, PRO312, LEU313, VAL319

and van der Waals interactions (hydrophobic contact) with TRP15, ALA292 and TRP343, a binding energy of − 7.47 kcal/mol. Meanwhile, compound **2** showed a binding affinity of − 5.54 kcal/mol for the hydrogen bonding interaction with LYS156, and van der Waals interactions involving TYR158, VAL232 and VAL313. Compound **3** showed a higher binding energy of − 10.19 kcal/mol with ARG335 interacting with the oxygen attached to the bis-acetyloxy group via hydrogen bonding; LYS156, TYR158, PRO312, PHE314, ARG315, and TYR316 residues interacted via hydrophobic contact. Despite only one residue interaction by a hydrogen bond to its hydroxyl group, compound **3** exhibited a better binding energy than the positive control. Meanwhile, compound **4** had a binding energy of − 8.31 kcal/mol where GLY209 interacted with a hydroxyl group via hydrogen bonding; VAL232, HIE280, VAL308, PRO312, LEU313 as well as VAL319 residues were found to interact via hydrophobic contact. The four compounds described above demonstrated a hydrophobic nature predominantly by interacting with the hydrophobic residues of the protein.

Fig. 4 shows the superimposed 3D diagram that represents the virtual binding site of the compound molecules in the enzymatic protein which predominantly exists in domain A; domain A has the catalytic region. The compound interaction mainly involves hydrophobic interactions; however, main residues residing at the entrance of the active site pocket are involved in the interaction. Overall, the interaction involves hydrogen bonding along with hydrophobic interactions such as van der Waals and π interactions, depending on the nature of residues interacting with the atoms and the nature of the compounds themselves.

4. Discussion

Various methods have been developed and applied to the extraction of natural products (i.e., plants and herbs) for use as alternatives to modern medicinal drugs. The most conventional method that has been used for decades is boiling or preparing a decoction with water, a rather simple and economically viable process. Recently, medicinal plant-based researches have been performed and many are on-going as a variety of metabolites with health benefits that have been found in plants. Nowadays, in more advanced researches, organic solvents are utilized to obtain plant extracts containing various metabolites, based on the polarity and nature of the compound(s) of interest [29]. Other factors that may influence the procedure used for plant extraction include the types of solvent to be used, nature of the plant material, temperature set during extraction and target metabolites [27]. The variation in solvent polarity results in bioactivities and phytochemical constituents that are remarkably different. Therefore, we used solvents of different polarity to obtain the leaf fractions from *C. nutans* in efforts to evaluate these different metabolites. From this, we found a variety of metabolites having different extents of bioactivity owing to their differences in solvent polarity.

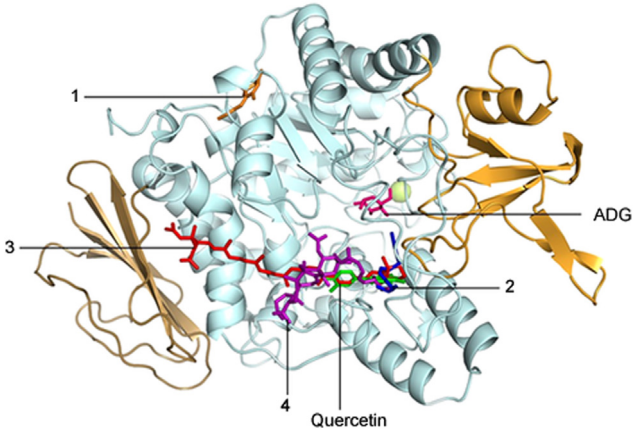

Fig. 4. The 3D diagram showing the superimposed binding site of compounds **1**, **2**, **3** and **4** with the receptor.

In vitro bioassay techniques serve as simple and rapid bench-top bioassay methods, as well as starting points for multidisciplinary efforts directed at drug discovery. The purpose of these bioassays is to rapidly screen and identify interesting biological activities so that more detailed mechanism-based studies of a multidisciplinary nature can follow [28]. Likewise, the α-glucosidase inhibition assay conducted was in efforts to assess the ability of the fractions from *C. nutans* leaves to inhibit an enzyme's activity. This inhibition would then reduce the breakdown of complex carbohydrates by cleaving oligosaccharides into monosaccharides, a process which could normalize hyperglycaemia [30]. The α-glucosidase inhibitory activity of the different fractions exhibited the following trend: H > HE > EA > EM > M (Table 1). As the polarity increased, we observed a subsequent significant decrease in the α-glucosidase inhibitory activity of the fractions obtained from *C. nutans* leaves. Hence, the non-polar and semi-polar solvents show a greater potential in extracting the bioactive compounds responsible for α-glucosidase inhibitory activity, when compared to the polar solvents [29]. The observed outcome was influenced by the variability of the metabolites extracted using solvents with different polarity. This indicates that the metabolites present within the fractions, belong to non-polar or semi-polar group such as the terpenoids, sterols and fatty acids. Importantly, these results agree with that reported by Lee et al. [6]. In the present study, a weak inhibitory activity (13.57%; IC_{50} value > 1000 μg/mL) was observed in the M fraction obtained from the *C. nutans* leaves. Apparently, the variations in polarity of the solvents used in this study may be responsible for the variations in the active constituents obtained from the extraction process. As previously mentioned, the good inhibitory activity depicted by the H fraction might be a result of the presence of non-polar compounds including terpenoids such as betulin, thus showing α-glucosidase inhibiting potential [30].

LC-MS-based metabolomics through PLS was able to pinpoint 4 compounds correlated with the α-glucosidase inhibitory activity

of this plant. The compounds that have been identified are some of the rare compounds that have not been researched extensively. Compound **1** is commonly known as megastigmatrienone-4 and is sometimes referred to as tabanone. Previously, tabanone was mentioned as a volatile compound responsible for aroma, particularly associated with tobacco [23]. Tabanone and its isomers are often used as food flavoring agents in a combined mixture. The compound is also mainly found in *Imperatacylindrica*, commonly known as the cogon grass, a traditional medicinal plant in Asia [31]. The study performed by Ayu et al. [32] showed that the plant extract exhibited no toxic effect on animals, and significantly increased glucose tolerance in diabetic rats. These authors concluded that the ethanolic extract of *Imperatacylindrica* leaves has significant antidiabetic activity in the alloxan-induced diabetes model. Therefore, this compound may have contributed to the antidiabetic effect exhibited by the plant.

Compound **2** belongs to the N-alkylamides, a secondary metabolite in plants that are classified using the structural classification system owing to their wide structural diversity. Essentially, the compound comprises an alkyl chain linked to an amine group via an amide bond. However, its presence in *C. nutans* was yet to be reported. Previously, this compound was abundantly found in *Achilleamillefolium* and *Achilleaptarmica*, plants belonging to the Asteraceae family. These plants are traditionally used for their various medicinal properties including their antidiabetic remedial effect [28].

Compound **3**, 1′,2′-bis(acetyloxy)-3′,4′-didehydro-2′-hydro-β, ψ-carotene is a carotenoid [33] with more than 40 carbons within its structure. Compound **3** contains a bis-acetyloxy group that are linked to an alkyl group. Compound **4**, 22-acetate-3-hydroxy-21-(6-methyl-2,4-octadienoate)-olean-12-en-28-oic acid however, belongs to the terpene group and has now been identified (via this study) in the *C. nutans* plant. Compound **4** has a cyclic structure with OH groups. Despite its previous identification, a review of its activities has never been performed; thus, we have conducted a research with this compound to present its bioactivity. Generally, except for their identification, no report has focused on the α-glucosidase inhibiting activity of these compounds.

Although the identified compounds were not individually tested to obtain the bioactivity observed in the *in vitro* assay, *in silico* computational analysis was performed. This analysis confirmed the bioactivity of these compounds by predicting the possible interaction between enzyme and inhibitors. Based on the results obtained, the compounds more likely to inhibit the enzyme's activity were identified; however, the strength of the activity cannot be portrayed using the *in silico* technique. Based on the binding affinity between the protein residues and the compound, the energy level showed the compounds' potential to inhibit the enzyme's activity. The compounds showed an interaction with different residues unlike the positive control or the control ligand, thus, indicated a possible allosteric inhibition site or a non-competitive inhibition mode.

The structure of *S. cerevisiae* isomaltase comprises 589 amino acids folded into three domains: A, B and C. Collectively, the residues from 1 to 113 and 190 to 512 are in domain A, while residues from 114 to 189 and 513 to 589 are found in domain B and domain C, respectively. Domain A is a catalytic domain containing catalytic residues such as ASP215, GLU277, and ASP352 located at the C-terminal. Besides the catalytic residues, ASP62, TYR72, and ARG442 are also located near the active site and are thus involved in the catalytic event. All residues interacting with ADG contribute to the actual catalytic reaction and its binding energy [29,30]. As shown in Table 3, ADG interacted with ASH215 (protonated ASP215), a conserved residue which acts as the catalytic nucleophile. ADG also formed a hydrogen bond with the GLH277 (protonated GLU277) residue that acts as the general acid-base catalytic residue. In addition, ADG interacted with ASP352, which is responsible for stabilizing the substrate during the catalytic event, to strengthen the acid-base hydrolysis reaction [16,29].

Virtually, the active site of isomaltase is occupied by five water molecules that influence the enzyme's activity. These water molecules will bind to some of the residues to ease the catalytic action. Precisely, water molecules will be arranged in a chain close to the bottom of the active site pocket and will form hydrogen bonds directly with ASP69, ARG446, and ASP409. These molecules also form an H-bond with the carbonyl oxygen atom in the GLU408 residue and the N atom in VAL410 and GLU408. H-bond formation by water molecules also involves the ARG213, GLU277,GLU349, and ASP352 residues. The surroundings of the binding site of water also have some hydrophobic amino acids such as TRP58, PHE301, PHE303, TYR347, TYR387, and TYR389. The presence of these hydrophobic residues is due to the hydrophobicity of the environment surrounding those water molecules that may increase their mobility. The actual role of these water molecules is to act as a reservoir to provide water for the subsequent catalytic reaction, and to function as a water drain at the active site to enhance substrate analogue binding. Therefore, despite the catalytic residues, the enzyme's activity also involves multiple other residues that may interact with inhibitors to cause non-competitive inhibition. In fact, the entrance of the active site pocket of isomaltase is shallow and primarily constricted by TYR158, HIS280, and loop 310–31 [29].

From the docking results, it is observed that all compounds are likely to form hydrophobic interactions with the residues of the enzymatic protein; thus, depicting their hydrophobicity. However, two of the compounds displayed good binding affinity with the residues involved, indicating their positive potential toward the observed bioactivity. These compounds were also comparably better in their binding energy level than quercetin. Overall, the interactions predominantly involved the residues residing in domains A and B. Interactions of compound **1** typically involve residues at domain A; however, these interactions are not with the actual catalytic residues. This suggests an indirect involvement of the compounds leading to the cessation of the enzymatic activity. Based on this prediction, this may also suggest that a non-competitive inhibition mode with an allosteric site interaction may have been adopted; however, further confirmation is required.

The rest of the compounds showed at least one interaction with the residues residing at the entrance of the active site pocket where TYR158 was found to interact with compounds **2** and **3**, and HIE280 with compound **4**. Such interaction results agree with the suggestion made by Yan et al. [30] that inhibitors may act non-competitively by interacting with the residues located at the entrance of the active site pocket. This may then lead to cleft closure to prevent the entrance of the substrate, which subsequently prevents enzyme activity. Additionally, these compounds were also observed to mainly interact with residues in domain A via hydrophobic interaction near the active site region. This suggests that the compounds are acting in a non-competitive inhibition mode to result in an inhibitory action [30]. In this study, the *in silico* docking simulation has provided supportive information that suggests the possible interaction between enzyme and the identified inhibitors, thus allowing us to predict the inhibition mode and activity of the compounds. Virtually, the enzyme-inhibitor complex can also be visualized using this technique. However, further investigations to assess the bioactivity of the identified compounds will serve as an added advantage to confirm their actual mechanism as well as their potential strength in the observed bioactivity.

All the compounds found in this study are likely to form hydrophobic interactions with the residues of the enzymatic protein. However, two of the compounds displayed a good binding affinity

with the bound residues. This indicated their positive potential toward the observed bioactivity as well as their theoretically better binding energy than that of quercetin. Overall, the interactions predominantly involved the residues residing in domains A and B. It was observed that compound **1** mainly interacted with residues at domain A; however, this interaction was not with the actual catalytic residues. This suggests the indirect involvement of the compounds leading to the cessation of enzymatic activity. Based on this prediction, we can also suggest that this may be a non-competitive inhibition mode with interaction at an allosteric site; however, further confirmation is required.

5. Conclusions

In the present study, the 4 compounds identified from the fractions collected from the *C. nutans* leaves were positively correlated with α-glucosidase inhibitory activity as shown via LC-MS-based metabolomics. The compounds identified were: (1) 4,6,8-Megastigmatrien-3-one; (2) N-Isobutyl-2-nonen-6,8-diynamide; (3)1′,2′-bis(acetyloxy)-3′,4′-didehydro-2′-hydro-β, ψ-carotene; and (4) 22-acetate-3-hydroxy-21-(6-methyl-2,4-octadienoate)-olean-12-en-28-oic acid. The *in silico* simulation study provided additional information for predicting the interaction between the inhibitors and enzyme. This information can serve as instructive data for future research involving the individual assessment of these compounds for their activity in a bioassay. Conclusively, *C. nutans* and its phytoconstituents can be further explored to develop novel antidiabetic agents to function as treatment and preventive measures for diabetes.

Acknowledgments

The authors wish to thank the Ministry of Agriculture of Malaysia for NKEA Research Grant Scheme fund (NRGS SP15-060-0182) and International Islamic University Malaysia for Publication Research Initiative Grant fund (PRIGS18-027-0027).

Conflicts of interest

The authors declare that there are no conflicts of interest.

References

[1] M. Bahmani, A. Zargaran, M.R. Kopaei, et al., Ethnobotanical study of medicinal plants used in the management of diabetes mellitus in the Urmia, Northwest Iran, Asian Pac. J. Trop. Med. 7 (2014) 348–354.
[2] T.E. Siong, R.Y.W. Kuan, Type 2 diabetes mellitus in Malaysia: current trends and risk factors, Eur. J. Clin. Nutr. 71 (2017) 844–849.
[3] S.M.N. Azmi, P. Jamal, A. Amid, Xanthine oxidase inhibitory activity from potential Malaysian medicinal plant as remedies for gout, Int. Food Res. J. 19 (2012) 159–165.
[4] A. Alam, S. Ferdosh, K. Ghafoor, et al., *Clinacanthusnutans*: a review of the medicinal uses, pharmacology and phytochemistry, Asian Pac. J. Trop. Med. 9 (2016) 402–409.
[5] S. Arullappan, P. Rajamanickam, N. Thevar, et al., In-vitro screening of cytotoxic, antimicrobial and antioxidant activities of *Clinacanthusnutans* (Acanthaceae) leaf extracts, Trop. J. Pharm. Res. 13 (2014) 1455–1461.
[6] S.Y. Lee, A. Mediani, N.A. Abdul-Hamid, et al., Antioxidant and α-glucosidase inhibitory activities of the leaf and stem of selected traditional medicinal plants, Int. Food Res. J. 21 (2014) 165–172.
[7] W.Y. Hung, C.W. Tun, W.C. Thin, et al., The use of calibration approaches for quantitative GC/MS analysis- secobarbital example, Forensic Sci. J. 5 (2006) 13–19.
[8] W. Liu, D. Yin, N. Li, et al., Influence of environmental factors on the active substance production and antioxidant activity in *Potentilla fruticosa* L. and its quality assessment, Sci. Rep. 6 (2016) 28591.
[9] R. Wang, Y. Lu, S. Wang, Comparative evaluation of 11 scoring functions for molecular docking, J. Med. Chem. 46 (2003) 2287–2303.
[10] N. Javadi, F. Abas, A.A. Hamid, et al., GC-MS-based metabolite profiling of *Cosmos caudatus* leaves possessing alpha-glucosidase inhibitory activity, J. Food Sci. 79 (2014) 1130–1136.
[11] J. Yang, Y.S. Kwon, M.J. Kim, Isolation and characterization of bioactive compounds from *Lepisorusthunbergianus* (Kaulf.), Arab J. Chem. 8 (2015) 407–413.
[12] A. Mediani, F. Abas, A. Khatib, et al., ^{1}H NMR-based metabolomics approach to understanding the drying effects on the phytochemicals in *Cosmos caudatus*, Food Res. Int. 49 (2012) 763–770.
[13] U. Lawal, S.W. Leong, K. Shaari, et al., α-glucosidase inhibitory and antioxidant activities of different *Ipomoea aquatica* cultivars and LC-MS/MS profiling of the active cultivar, J. Food Biochem. 41 (2016) 1–8.
[14] S. Aykul, E. Martinez-Hackert, Determination of half-maximal inhibitory concentration using biosensor-based protein interaction analysis, Anal. Biochem. 508 (2016) 97–103.
[15] T. Pluskal, S. Castillo, A. Villar-Briones, et al., MZmine 2: modular framework for processing, visualizing, and analyzing mass spectrometry-based molecular profile data, BMC Bioinforma. 11 (2010) 1–11.
[16] S.H. Seong, A. Roy, H.A. Jung, et al., Protein tyrosine phosphatase 1B and α-glucosidase inhibitory activities of *Puerarialobata* root and its constituents, J. Ethnopharmacol. 194 (2016) 706–716.
[17] P. Banerjee, J. Erehman, B.O. Gohlke, et al., Super Natural II – a database of natural products, Nucleic Acids Res. 43 (2015) 935–939.
[18] W. Lestari, R.T. Dewi, L.B.S. Kardono, et al., Docking sulochrin and its derivative as α-glucosidase inhibitors of *Saccharomyces cerevisiae*, Indones, J. Chem. 17 (2017) 144–150.
[19] T.J. Dolinsky, J.E. Nielsen, J.A. Mc Cammon, et al., PDB2PQR: an automated pipeline for the setup of Poisson-Boltzmann electrostatics calculations, Nucleic Acids Res. 32 (2004) 665–667.
[20] K. Wang, L. Bao, K. Ma, et al., A novel class of α-glucosidase and HMG-CoA reductase inhibitors from *Ganodermaleu cocontextum* and the anti-diabetic properties of ganomycin I in KK-Aymice, Eur. J. Med. Chem. 127 (2017) 1035–1046.
[21] R.Y. Nsimba, H. Kikuzaki, Y. Konishi, Antioxidant activity of various extracts and fractions of *Chenopodium quinoa* and *Amaranthus* spp. seeds, Food Chem. 106 (2008) 760–766.
[22] Database of Multi- and Megavariate Data Analysis, Basic Principles and Applications, Third revised edition, Chapter 18, Umetrics Academy, 2013: 323–355. ⟨https://pdfs.semanticscholar.org/045f/6250ad3a3e1c5337f4859c4464617926cd5c.pdf⟩.
[23] J. Cai, B. Liu, P. Ling, et al., Analysis of free and bound volatiles by gas chromatography and gas chromatography-mass spectrometry in uncased and cased tobaccos, J. Chromatogr. A 947 (2002) 267–275.
[24] D. Slaghenaufi, M.C. Perello, S. Marchand-Marion, et al., Quantitative solid phase microextraction - gas chromatography mass spectrometry analysis of five megastigmatrienone isomers in aged wine, Anal. Chim. Acta 813 (2014) 63–69.
[25] Y.S. Alagar, S. Ramalingam, A. Jebamalairaj, et al., Biochemical fingerprint and pharmacological applications of *Barlerianoctiflora* L.f. leaves, J. Complement. Integr. Med. 13 (2016) 365–376.
[26] J. Boonen, B. Baert, C. Burvenich, et al., LC-MS profiling of N-alkylamides in *Spilanthesacmella* extract and the trans mucosal behaviour of its main bioactive spilanthol, J. Pharm. Biomed. Anal. 53 (2008) 243–249.
[27] F. Mbeunkui, M.H. Grace, C. Lategan, et al., Isolation and identification of antiplasmodial N-alkylamides from *Spilanthesacmella* flowers using centrifugal partition chromatography and ESI-IT-TOF-MS, J. Chromatogr. B 879 (2011) 1886–1892.
[28] L. Veryser, L. Taevernier, E. Wynendaele, et al., N-alkylamide profiling of *Achilleaptarmica* and *Achilleamillefolium* extracts by liquid and gas chromatography–mass spectrometry, J. Pharm. Anal. 7 (2017) 34–47.
[29] K. Yamamoto, H. Miyake, M. Kusunoki, et al., Crystal structures of isomaltase from *Saccharomyces cerevisiae* and in complex with its competitive inhibitor maltose, FEBS J. 277 (2010) 4205–4214.
[30] J. Yan, G. Zhang, J. Pan, et al., α-Glucosidase inhibition by luteolin: kinetics, interaction and molecular docking, Int. J. Biol. Macromol. 64 (2014) 213–223.
[31] H.J. An, A. Nugroho, B.M. Song, et al., Isoeugenin, a novel nitric oxide synthase inhibitor isolated from the rhizomes of *Imperatacylindrica*, Molecules 20 (2015) 21336–21345.
[32] S.A. Ayu, B.S. Samsul, F. Santosh, et al., Antidiabetic activity of ethanolic extract of *Imperata cylindrical* (lalang) leaves in alloxan induced diabetic rats, Arch. Pharm. Pract. 3 (2012) 46.
[33] H. Ronneberg, A.G. Andrewes, G. Borch, et al., CD correlation of C-2′ substituted monocyclic carotenoids, Phytochemistry 24 (1985) 309–319.